# Reverberation Suppression Using Wideband Doppler-Sensitive Pulses

Yves Doisy, Laurent Deruaz, Sander P. van IJsselmuide, S. Peter Beerens, and Robert Been

***Abstract*—The influence of transmitted waveforms on the signal-to-reverberation ratio (SRR) of a low-frequency active sonar is analyzed both theoretically and experimentally. Reverberation experiments have been conducted during a sea trial in a littoral water environment in October 1999. The aim of the trials was to compare the performance of three classes of waveforms: standard hyperbolic frequency-modulated (HFM) waveforms, continuous waveforms (CWs), and innovative pulse trains of linear frequency-modulated (PTFM) waveforms. Transmissions were combined (CW/PTFM train) or intermitted (HFM) to compare the performance of the three classes in (exactly) the same environment. Experimental results in highly reverberant environment illustrated that PTFM pulses allow a reduction in reverberation power greater than 10 dB over the standard detection pulses for slowly moving targets. The results are in agreement with theoretical predictions.**

***Index Terms*—Active sonar, Doppler, matched filter, reverberation, sonar waveforms.**

## I. Introduction

### A. Background

LOW-FREQUENCY active sonar (LFAS) is a very promising sensor for the detection of modern quiet submarines, which has currently become increasingly problematic. The Physics and Electronics Laboratory of The Netherlands Organization for Applied Scientific Research (TNO, The Hague, The Netherlands) and Thales Underwater Systems SAS (TUS SAS, Sophia-Antipolis, France) have initiated a collaborative research program in this field, which is named the New Array Technology II (NAT II) program.

The goal of the NAT II program is to improve detection performance of LFAS systems in shallow-water environments. Therefore, the following two main research themes are defined:

- port/starboard (P/S) discrimination;
- reverberation suppression.

Some results of the study on the latter theme are discussed in this paper. Reverberation suppression is of great interest in shallow-water antisubmarine warfare (ASW) operations with LFAS systems. Reverberation from bottom structures masks possible target detection and creates innumerable false alarms. For a proper definition of reverberation, we quote the introduction to this topic in the famous book of Urick [1, p. 237]:

> The sea contains, within itself and on its boundaries, inhomogeneities of many different kinds, varying in size from schools of fish to seamounts and coastal slopes. These inhomogeneities form discontinuities in the physical properties of the medium and thereby intercept and re-radiate a portion of the acoustic energy which is incident upon them. This radiated sound is called scattering, and the sum of these scatterings is known as reverberation. It is heard as a long, slowly decaying, quivering tonal blast following the transmission of an active sonar system.

### B. Means for Reverberation Suppression

Reverberation can be reduced both by a proper choice of the transmitted signal and by suitable array and signal processing. In this paper, we focus on the influence of transmitted signals on reverberation suppression, assuming conventional beamforming and replica correlation are performed on the receiver side.

To suppress reverberation from the receiver side, it is important that the LFAS array has a beampattern [2] with the following properties:

- P/S discrimination;
- narrow beamwidth;
- low sidelobes.

P/S discrimination is of utmost importance for operations in coastal areas, as we will show later in this paper. Reverberation from a coastal slope can be very severe and to reject this, a strong (20 dB or more) P/S discrimination is required. This may prevent that this coastal reverberation leaks into offshore bearings and masks detection there. The topic of P/S discrimination is one of the main themes of the NAT II program and is treated in great detail in an accompanying paper [3].

Influence of beamwidth and sidelobe levels on the reverberation level strongly depends on the nature of the transmitted pulse and on target radial speed and will be discussed in Section II. When operating on a moving platform, the reverberation power in Doppler mode for moving targets is governed by sidelobe levels, the mainlobe beamwidth having no influence. Also, in case of directional (coastal) reverberation, a reduction of sidelobes can be more effective than decreasing the beamwidth. Therefore, it is advised to apply shading to the array in reverberant areas.

Manuscript received April 27, 2006; revised June 20, 2008; accepted July 08, 2008. Current version published February 06, 2009. This work was supported by the Dutch and French MoD, represented by the Royal NetherLands Navy (RNLN) and the Delegation Generale pour l'Armement (DGA), respectively.

**Associate Editor: D. A. Abraham**.

Y. Doisy and L. Deruaz are with Thales Underwater Systems SAS, BP 157, 06903 Sophia-Antipolis, France (e-mail: yves.doisy@fr.thalesgroup.com; Laurent.Deruaz-Pepin@fr.thalesgroup.com).

S. P. van IJsselmuide and S. P. Beerens are with the Physics and Electronics Laboratory (FEL), The Netherlands Organization for Applied Scientific Research (TNO), 2509 JG The Hague, The Netherlands (e-mail: sander.vanijsselmuide@tno.nl; peter.beerens@tno.nl).

R. Been is with the Netherlands Organization for Applied Scientific Research (TNO), Physics and Electronics Laboratory (FEL), 2509 JG The Hague, The Netherlands, and also with NATO Undersea Research Centre (NURC), 19126 La Spezia, Italy (e-mail: Been@nurc.nato.int).

Digital Object Identifier 10.1109/JOE.2008.2002582

To suppress reverberation from the transmitter side, it is important that the LFAS transmits suitable waveforms. Vertical directivity of the source can also decrease reverberation, and limit the Doppler spreading of reverberation, but with limited efficiency at long ranges.

### C. Outline of the Paper

In Section II, sonar waveforms are introduced and discussed. Classes of waveforms are introduced and an overview and summary of the reverberation theory for continuous waveforms (CWs), pulse train of frequency-modulated (PTFM) signal, and hyperbolic frequency-modulated (HFM) signal are given. Expressions for the reverberation levels of the three classes of LFAS pulses are derived. In Section III, the reverberation experiments of the NAT 1999 trial are described. In that trial, the Combined Active and Passive Towed Array Sonar (CAPTAS) was operated in an extremely rich clutter area against a real and an artificial target. Analysis results for the three classes of pulses are given in Section IV. The experimental results for the reverberation levels are compared to the theoretical results obtained in Section II. Finally, the findings are discussed in the conclusion of this paper in Section V.

## II. Overview of LFAS Waveforms and Reverberation Theory

In this section, active sonar waveforms are discussed and classes of waveforms are defined according to their performances in the reverberation-limited environment. The waveforms are first introduced and their properties analyzed in terms of ambiguity function. In the second part of this section, expressions for signal-to-reverberation ratio (SRR) at processing output for a sonar moving at constant speed are derived, and are shown to be determined by the waveform spectrum. Three classes of waveforms are defined according to the shape of their spectrum and performances are discussed in each case.

### A. Overview of LFAS Waveforms

The choice of the pulse with best performance in a given environment depends on the background (noise or reverberation) and on the motion of the target. The performance in noise is mainly connected to the energy of the transmitted pulse, while the performance in reverberation is governed by the ambiguity function of the pulse. The ambiguity function gives the matched-filter output of a pulse as a function of range and Doppler; see, e.g., [4] and [5]. The reverberation level at the output of the replica correlation (matched to the hypothesized target speed) is given by the integral over time (or range) of the ambiguity function. For a pulse of a given energy, the total volume under the ambiguity function is fixed. Therefore, the design of a pulse is a matter of operational choice of where to concentrate the ambiguity volume, e.g., along the range or Doppler axis. More insight can be gained by considering the pulse spectra, where as shown in Section II, the reverberation level is given by the integral over frequency of the cross-spectral intensity between the transmitted pulse and its Doppler scaled version (corresponding to the hypothesized replica of the target). Pulses with high bandwidth have lower spectral level (or smaller resolution cells) than pulses with lower bandwidth, but have larger overlap in frequency. Therefore, the level of reverberation is governed both by bandwidth and by overlap of the pulse spectrum and its Doppler scaled version.

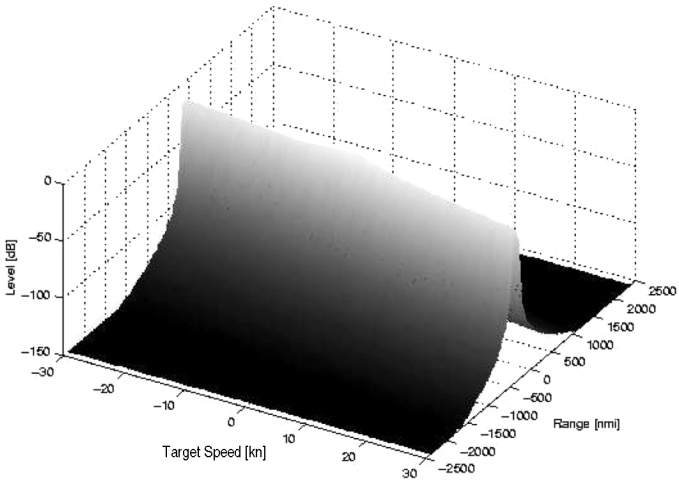


Fig. 1. Ambiguity surface of a 4-s, 500-Hz HFM pulse.

*1) Wideband Flat Spectrum Pulses:* These pulses have a flat spectrum amplitude over the bandwidth $B$. They are based on the idea that high bandwidth and pulse compression (in the matched filter) yield a high range resolution. The square magnitude of their spectrum is low (proportional to $T/B$, where $T$ is the duration of the pulse). Several pulse types belong to this class, depending on the phase modulation of the spectrum. The HFM pulse, also known as linear period modulation (LPM) is mostly used in sonar applications for its Doppler insensitivity, allowing to process all Doppler targets with only one replica; see Fig. 1 for a typical ambiguity function of an HFM pulse.

Other waveforms with flat spectrum amplitude have various Doppler sensitivity (e.g., Doppler measuring frequency-modulated (DMFM) waveforms, binary phase-shift keying waveforms (BPSK), pseudorandom noise waveforms (PRN), nonlinear frequency-modulated waveforms (NLFM), Costas; see [6]–[10]). The Doppler sensitivity of these pulses is tunable, but still these do not allow to suppress reverberation by means of Doppler filtering. This is because the frequency shift of the target replica spectrum is usually much smaller than the transmitted bandwidth, and therefore, the overlap between the transmitted (reverberation) spectrum and the Doppler scaled (target) spectrum is unaffected by the motion of the target. In some situations, however, Doppler sensitivity is of great value for classification purposes.

Also, the famous linear frequency-modulated (LFM) pulse belongs to this category, but this pulse has become recently unpopular in the LFAS world, because its Doppler sensitivity is not tunable and increases with bandwidth; see, e.g., [11] and [12].

*2) Continuous-Wave Pulses:* This signal is a tone of frequency $f$ and a duration $T$. Generally, its amplitude is weighted to allow control of spectral sidelobes. They are designated hereafter as weighted continuous wave (WCW). The transmitted pulse has a high spectral amplitude (taken as 1 for reference), and narrow spectral width, proportional to $1/T$; see, for instance, Fig. 2 for a typical ambiguity function of a WCW pulse.

For targets with Doppler shift larger than $1/T$, the overlap of the spectra between reverberation and replica is very small

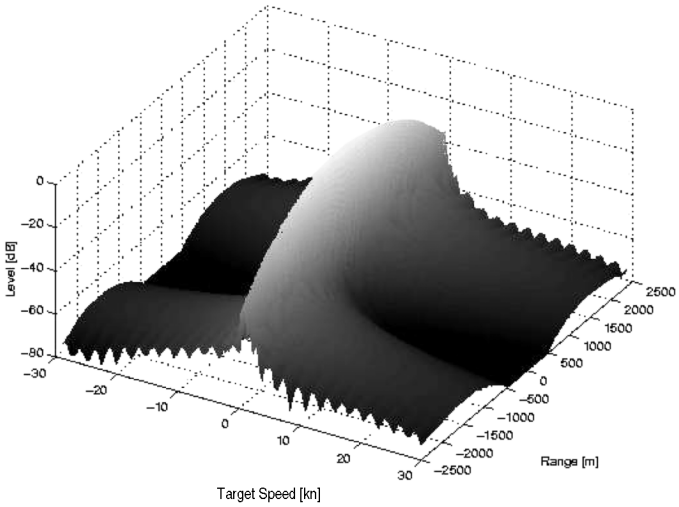


Fig. 2. Ambiguity surface of a 4-s, 1088-Hz weighted CW pulse.

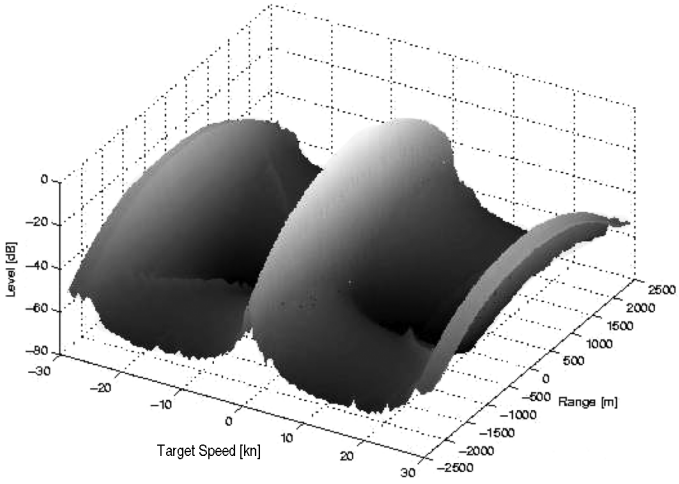


Fig. 3. Ambiguity surface of a 4-s, 700-Hz PTFM pulse with 128 subpulses.

and reverberation is rejected by Doppler filtering. However, the transmitted bandwidth is narrow as compared to HFM, resulting in a very large resolution cell (several miles for typical LFAS pulse durations). In the presence of Doppler spreading due to tow-ship motion, the rejection is also limited by the sidelobes of the array beampattern (see Section II) and the Doppler rejection hardly compensates for this loss of bandwidth, except for target echoes whose frequency lays outside the spectrum of reverberation, which corresponds to the zone C defined in Section II.

*3) Wideband Comb Spectrum Pulses:* These pulses aim at combining Doppler filtering of reverberation and the advantages of high bandwidth. They occupy all the available bandwidth, with a spectrum made of spikes of width $1/T$, separated by regions of low sidelobes. Examples are the "Cox comb" pulses (sum of CW pulses with different center frequencies), the sinusoidal FM pulses (SFM), which are the periodically swept FM pulses, and the pulse trains of FM sweeps (PTFM); see, e.g., [13]–[15]. Cox comb pulses are limited in amplitude (beating effects) and perform poorly in noise. In this paper, the PTFM pulse is selected for further analysis. The intensity of the spectrum on the spikes is intermediate between HFM and WCW ($N/BT$ for a PTFM of $N$ FM subpulses of bandwidth $B$ and duration $T$), but for targets within Doppler shifted larger than $1/T$, the overlap of the spectra between reverberation and replica is very small and reverberation is rejected by Doppler filtering. A typical ambiguity function of a PTFM pulse can be seen in Fig. 3.

Fig. 3 clearly shows the "trick" that the wideband PTFM pulse plays with the ambiguity function. At low target speeds ($V_r <$ 16 kn), the ambiguity function resembles the ambiguity function of the CW pulse. However, at higher target speeds, the ambiguity function rises again. Because the total volume under the surface must be one, these Doppler "sidelobes" make it possible to obtain lower sidelobes at the low target speeds.

### B. Reverberation Theory

In this section, an overview and summary of reverberation theory is given. First, we start with a general expression of the signal and the reverberation level at the output of the signal processing, i.e., beamforming and matched filtering. This general expression is applied to compute the gain in SRR of special waveforms compared to the classical CW and FM waveforms. The theory in this section is based on several conference papers [16]–[18].

For the definition of the signal and the reverberation level, straightforward signal processing is assumed, which consists of the following:

- shaded normalized beamforming, where the array beampattern of a beam steered in direction $\theta$ is denoted $b(\theta)$;
- replica correlation in each beam with a set of normalized Doppler scaled replicas $e(\alpha t)$ of the transmitted waveform, where $e(t)$ stands for the analytical signal.

Reduction of processing gain due to coherence losses (spatial and temporal) is neglected throughout this paper. Furthermore, it is assumed that the sonar consists of an omnidirectional source and a linear towed array receiver, traveling at a constant speed $\vec{V}$. The source transmits signals of duration $T$, at a center frequency $f_0$ and bandwidth $B$. The total transmitted energy for a signal with analytic nondimensional waveform $e(t) = \mathrm{a}(t)\exp[\imath\phi(t)]$ (where $\mathrm{a}(t) \leq 1$ for $0 \leq t \leq T$ and 0 elsewhere, and where $\phi(t)$ is the phase law of the code), is given by

$$E_T = \frac{1}{2}\int_t |e(t)|^2 \,\mathrm{d}t. \tag{1}$$

The received signal (reflected from the target) on the array after (shaded) beamforming and replica correlation (tuned to the target Doppler) is proportional to

$$s = b(\theta_0)\int_t |e(\alpha_0 t)|^2 \,\mathrm{d}t \tag{2}$$

and the corresponding signal power is given by

$$S = |s|^2 = \left| b(\theta_0)\int_t |e(\alpha_0 t)|^2 \,\mathrm{d}t \right|^2. \tag{3}$$

In (3), the terms related to the source level, the propagation loss, and the target strength are not shown. The term $b(\theta_0)$ is the

normalized beamformer output, which is one for target direction $\theta_0$. The last term represents the effect of replica correlation. The matched-filter output depends on the target Doppler by means of the time-compression factor $\alpha_0 = 1+2V\cos(\theta_0)/c+2V_r/c$, in which $V_r$ is the (absolute) target radial speed, $V$ is the magnitude of the sonar speed, and $\theta_0$ is the bearing of the target (the angle between target direction and own ship speed direction).

The reverberation power at the output of the beam and replica matched to the target, scaled as in (3), assuming a homogeneous distribution of uncorrelated scatterers in a plane of the array, is given by (see [19, Sec. 12.3.2])

$$R_R = \int_{\theta=0}^{2\pi} |b(\theta)|^2 \left[ \int_t |C_{\alpha_\theta,\alpha_0}(t)|^2 \,\mathrm{d}t \right] \mathrm{d}\theta. \tag{4}$$

In (4), the terms related to the source level, the propagation loss, and the scatterer strength are not shown. The integration over time and direction (bearings) covers the contributions of all scatterers spread on the surface around target range. Replica correlation is represented by

$$C_{\alpha_\theta,\alpha_0}(t) = \int_u e(\alpha_\theta u) e\,(\alpha_0(u+t))^* \,\mathrm{d}u \tag{5}$$

where $C_{\alpha_\theta,\alpha_0}$ is the correlation function between the replica matched to the target Doppler and the reverberation scatterers in direction $\theta$. For an array towed with a constant speed $V$, the scatter Doppler parameter $\alpha_\theta$ depends only on the scatter bearing $\theta$ with respect to the array and reads: $\alpha_\theta = 1 + 2V\cos\theta/c$. In reverberation-limited situations, the SRR determines the detection performance of the sonar system. In these situations, one should maximize this ratio, or in other words, minimize $R_R/S$. This is in contrast to the noise-limited situations, where the transmitted energy $E_T$ should be maximized for a better signal-to-noise ratio (SNR). The objective of a waveform design is to minimize the ratio $R_R/S$, which is the inverse of the SRR, without compromising in $S$ (and thus $E_T$). This reverberation-to-signal ratio (RSR) has the following form:

$$\mathrm{RSR} = \frac{\int_{\theta=0}^{2\pi} |b(\theta)|^2 \left[ \int_t |C_{\alpha_\theta,\alpha_0}(t)|^2 \,\mathrm{d}t \right] \mathrm{d}\theta}{\left| \int_t |e(\alpha_0 t)|^2 \,\mathrm{d}t \right|^2}. \tag{6}$$

The matched-filter output in (5) is simplified by application of Parseval's theorem. This leads to the following expression for the RSR:

$$\mathrm{RSR} = \frac{\int_{\theta=0}^{2\pi} |b(\theta)|^2 \left[ \int_f |E_\theta(f) E_0(f)|^2 \,\mathrm{d}f \right] \mathrm{d}\theta}{S} \tag{7}$$

where $E(f)$ is the spectrum of the transmitted pulse

$$E_0(f) = \int e(\alpha_0 t) e^{-i2\pi f t} \mathrm{d}t = E(f/\alpha_0)/\alpha_0 \simeq E(f/\alpha_0)$$

$$E_\theta(f) = \int e(\alpha_\theta t) e^{-i2\pi f t} \mathrm{d}t = E(f/\alpha_\theta)/\alpha_\theta \simeq E(f/\alpha_\theta)$$

where we have taken into account the fact that sonar and target speeds are small with respect to sound speed to approximate $\alpha_\theta$ and $\alpha_0$ by 1. In the following sections, the general equation for the average RSR is computed for the different waveforms. This enables us to compare the waveform performance in the reverberation-limited situations quantitatively.

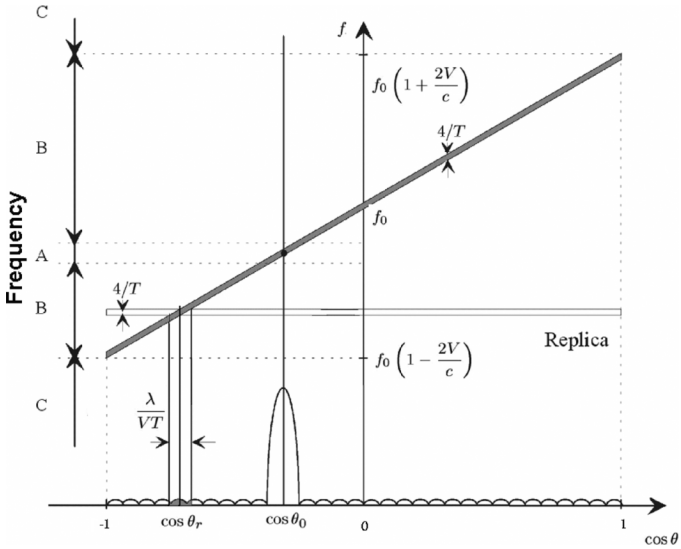


Fig. 4. Reverberation zones for a CW pulse.

### C. Continuous-Wave Signals

A CW, or to suppress spectral sidelobes, preferably a weighted CW, is used for a Doppler detection. The weighted CW is a monotonic pulse and can be described as

$$e(t) = \sin^2\left(\pi \frac{t}{T}\right) \exp(2\pi\imath f_0 t), \qquad \text{for} \quad 0 \le t \le T. \tag{8}$$

The choice of the exact shading law is a matter of a tradeoff between Doppler resolution and transmit energy (for performance in noise-limited environment) on the one hand, and spectral sidelobe level (which should be low to avoid the contribution from reverberation in the same bearing as the target but at different frequencies, as discussed below) on the other hand. Using a $\sin^2$ or a Hamming shading, the total width between nulls of the pulse spectrum is $4/T$.

Graphical interpretation of the reverberation level, based on the integral in (4), is given in Fig. 4 (cf., [16]).

The vertical axis corresponds to frequency, and the horizontal axis to the cosine of the bearing $(\cos\theta)$, so that the reverberation spectrum corresponds to a single line in this representation, described by

$$f = f_0\left(1 + \frac{2V}{c}\cos\theta\right). \tag{9}$$

From Fig. 4, three reverberation zones can be classified in the Doppler spectrum of reverberation at the output of beamforming. These zones are named zone **A**, **B**, and **C** and they correspond to very low, low, and high Doppler targets, respectively. Very low Doppler targets are targets with radial speed such that the Doppler shift of their spectrum falls within the Doppler spread of reverberation induced by the scatterers within the mainlobe of the beampattern. High Doppler targets mean that the target radial speed is such that there is no scatter matching the Doppler shift of their spectrum. Low Doppler

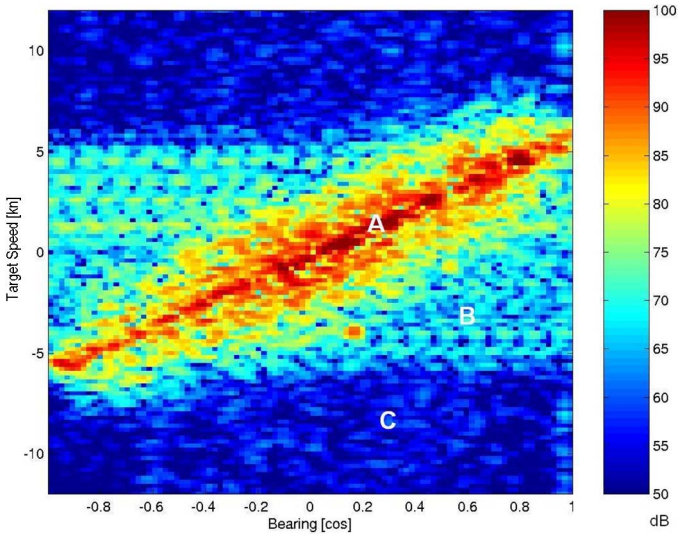


Fig. 5. Example of reverberation zones for a WCW pulse.

targets (zone **B**) are such that the Doppler shift of their spectrum matches the Doppler spectrum of scatterers attenuated by the sidelobes of the beampattern. The frequency limits of these three zones depend on the beam steering direction. In Fig. 5, a typical example of the three reverberation zones after Doppler processing of a transmitted CW pulse is shown for all the beams. This bearing–Doppler plot clearly demonstrates the problems that occur in zones **A** and **B**. High-reverberation levels in zone **A** are clearly recognizable by the red colored slant line between Dopplers of 6 and $-6$ kn, which has a slope according to (9). Zone **B** is characterized by the yellow band in the same Doppler bracket and it covers all bearings. The blue area outside the Doppler bracket of zone **A** and **B** corresponds to the low-reverberation levels in zone **C**.

In the following subsections, the performance of the (weighted) CW pulse in each of these three reverberation zones is discussed.

*1) Zone* **A** *Performance:* In this zone, part of the cross spectrum between the replica and the reverberation signals falls in the mainlobe of the beampattern (mainlobe is considered between the first nulls of the beampattern). This means that the corresponding Doppler channel is associated to scatterers in the direction of the beam. These scatterers are rejected neither by the beampattern nor by the Doppler filter. It is clear that the CW performance in the reverberation-limited conditions is very poor in zone **A**. We will first identify zone **A** for our application and then determine the reverberation levels in that zone.

From Fig. 4, it can be seen that zone **A** corresponds to the following range of target radial speed:

$$\begin{aligned}\left(1+\frac{2V\cos\theta_0}{c}+\frac{2V_r}{c}\right)f_0+\frac{2}{T}&\le\left(1+\frac{2V\cos\theta_0^{(-)}}{c}\right)f_0-\frac{2}{T}\\ \left(1+\frac{2V\cos\theta_0}{c}+\frac{2V_r}{c}\right)f_0-\frac{2}{T}&\ge\left(1+\frac{2V\cos\theta_0^{(+)}}{c}\right)f_0+\frac{2}{T}\end{aligned}\tag{10}$$

where $\theta_0^{(-)}$ and $\theta_0^{(+)}$ are the bearings of the first nulls of the beampattern (respectively, to the left and to the right of the maximum on 4), and $\theta_0$ is the bearing of the beam steered on the target. For a linear receiving array of length $L$, the beamwidth in $\cos(\theta)$ unit between the maximum and the first null is

$$\left|\cos\theta_0^{(\pm)}-\cos\theta_0\right|=\beta\frac{\lambda_0}{L}$$

where $\beta$ is a coefficient depending on the shading of the array ($\beta=1$ for a rectangular shading and $\beta=2$ for Hamming shading [20]). For a broadside, the target speed range associated to "zone **A**" reads

$$-V\frac{\beta\lambda_0}{L}-\frac{2\lambda_0}{T}\le V_r\le V\frac{\beta\lambda_0}{L}+\frac{2\lambda_0}{T}.\tag{11}$$

Now we return to the RSR as determined in (7). For a transmitted WCW, we have

$$E_0(f_0)=\int_0^T\sin^2\left(\frac{\pi t}{T}\right)\mathrm{d}t=\frac{T}{2}$$

and

$$S=\left[\int_0^T\sin^4\left(\frac{\pi t}{T}\right)\mathrm{d}t\right]^2=\frac{9T^2}{64}.\tag{12}$$

For zone **A** reverberation, the reverberation signal has the same Doppler (or frequency) as the target. Therefore, the integral for the reverberation level at the numerator of (7) can be approximated by

$$\int_f|E_\theta(f)E_0(f)|^2\,\mathrm{d}f\approx\left(\frac{T}{2}\right)^2\left(\frac{T}{2}\right)^2\frac{1}{T}=\frac{T^3}{16}.\tag{13}$$

The integral over the beampattern in (7) is determined by the $-3$-dB width $2\theta_3$ of the mainlobe of the beampattern,[1] resulting in the following expression for the RSR:

$$\mathrm{RSR}\simeq\frac{4}{9}T2\theta_3.\tag{14}$$

Numerical evaluation of (12) and (13) leads to a similar expression where the coefficient 4/9 is replaced respectively by 0.667 for rectangular shading, 0.527 for Hamming shading, and 0.481 for $\sin^2$ shading. As we consider either Hamming or $\sin^2$ shading in this paper, we will use the following expression:

$$\mathrm{RSR}\simeq\frac{1}{2}T2\theta_3.\tag{15}$$

The resulting reverberation levels for WCW in zone **A** are high, mainly because no gain from the matched filter is obtained. Increasing the pulse duration makes the result even worse; this increases the effective scattering surface (reverberation cell) and affects the signal and the reverberation strength in equal way.

[1]It is assumed here that the width $\Delta\theta$ defined in (18) is much larger than the beamwidth of the array $2\theta_3$. In the opposite case, $\Delta\theta$ should be substituted to $2\theta_3$ in (15), and in the intermediate case, the exact calculation of (7) has to be carried out.

Detection of still targets in reverberation-limited conditions will be difficult if not impossible with WCW pulses.

*2) Zone* $\mathbf{B}$ *Performance:* In zone $\mathbf{B}$, the cross spectrum between the replica and the reverberation signal falls in front of the beampattern sidelobes. This corresponds to the following range of radial target speeds:

$$\begin{aligned} V\frac{\beta\lambda_0}{L}+\frac{2\lambda_0}{T} \le V_r \le V(1-\cos\theta_0)+\frac{2\lambda_0}{T} \\ \text{(Zone A boundary)} \qquad\qquad \text{(Zone C boundary)} \\ -V(1+\cos\theta_0)-\frac{2\lambda_0}{T} \le V_r \le -V\frac{\beta\lambda_0}{L}-\frac{2\lambda_0}{T}. \\ \text{(Zone C boundary)} \qquad\qquad \text{(Zone A boundary)} \end{aligned} \tag{16}$$

It turns out that this is the most likely situation in ASW operations. Frigates will often search at a speed that is considerably larger than the speed of hostile submarines. Therefore, this zone is of particular interest.

In zone $\mathbf{B}$, there are two main contributions to the reverberation level, as can be seen from Fig. 4, which is the graphical representation of the integral in (7). The first contribution arises from the part of the bearing-frequency plane not attenuated by the beampattern. In this part, spectra of the replica and the reverberation overlap through their sidelobes, so that the integral of the cross spectra over frequency in (7) will be strongly attenuated. Physically, this contribution is associated to scatterers in the mainlobe of the beampattern, but at different frequencies (Doppler) than the target. The spectral sidelobes of a weighted CW pulse can reach $-50$ dB. This contribution is, therefore, most of the times negligible compared to the second contribution described below. The second contribution arises from the area of the bearing-frequency plane where the mainlobes of reverberation and replica spectra intersect. This area corresponds to directions outside the mainlobe of the beampattern, as shown in Fig. 4 for bearing $\theta_r$, so that the integral over bearing in (7) will be attenuated by the beampattern sidelobes. Physically, this contribution corresponds to the scatterers at the same frequency as the target, but at a different bearing. The beampattern sidelobes are generally much higher than the spectral sidelobes, even for a strongly shaded array, as they are limited by the phase and amplitude dispersions of the sensors whose effect is to generate a constant spatial background as shown in [21]. The contribution of the remaining part of the bearing-frequency plane in (7) is attenuated by both the spectral and spatial sidelobes and is neglected. To assess the reverberation level associated to the contribution of scatterers at the same frequency as the target, but at a different bearing, the angular interval $\Delta\theta$ corresponding to the overlap between the replica and the reverberation spectra must be worked out. This interval corresponds to the scatterers whose frequencies match the frequencies of the target Doppler channel. The center of this angular interval is the bearing $\theta_r$ such that

$$1+\frac{2V_r}{c}+\frac{2V}{c}\cos(\theta_0)=1+\frac{2V}{c}\cos\theta_r.$$

The $-3$-dB spectral width of the WCW is about $2/T$, so that the angular interval $\Delta\theta$ is given by

$$\frac{2V}{\lambda_0}\left[\cos\left(\theta_r-\frac{\Delta\theta}{2}\right)-\cos\left(\theta_r+\frac{\Delta\theta}{2}\right)\right]=\frac{2}{T}. \tag{17}$$

If $\Delta\theta$ is small, (17) is approximated by

$$\Delta\theta \approx \frac{\lambda_0}{VT\sin\theta_r}. \tag{18}$$

Equation (18) shows that the angular interval is inversely proportional to the tow speed and pulse length, and corresponds to the resolution of an array of length $VT$.

Graphical evaluation of (7) leads to the following expression for the RSR in $\mathbf{B}$ zone

$$\mathrm{RSR} \simeq \frac{4}{9}T\Delta\theta 10^{-\frac{\mathrm{SLL}}{10}}. \tag{19}$$

A numerical evaluation of (6) leads to similar expression with coefficient 4/9 replaced respectively by 0.50 for the rectangular and Hamming shadings and 0.481 for the $\sin^2$ shading. We will use the following expression:

$$\mathrm{RSR} \simeq \frac{1}{2}T\Delta\theta 10^{-\frac{\mathrm{SLL}}{10}} \tag{20}$$

where SLL is the beam sidelobe level averaged over the angular interval $\Delta\theta$, in decibels. When the sidelobes are limited by the phase and amplitude dispersions of the sensors, they can be assumed constant. The last term in (20) represents the sidelobe suppression of the beamformer. Reverberation in the Doppler channel of the target comes from the scatterers at other bearings where $f_r = (1+(2V/c)\cos\theta_r)f_0)$ and is suppressed by the beamforming. So, in a reverberation-limited situation, a long well-calibrated array is required to make the SLL low enough to provide sufficient SRR in zone $\mathbf{B}$. Note that because $T\Delta\theta$ is (almost) independent of $T$, the detection performance of WCW against slowly moving targets is independent of the pulse duration.

*3) Zone* $\mathbf{C}$ *Performance:* In zone $\mathbf{C}$, there is no scatter at the frequency of the target Doppler channel. This corresponds to the following target radial speeds:

$$\begin{aligned} -V\left(1+\cos(\theta_0)\right)-\frac{2\lambda_0}{T} \ge V_r \\ V_r \ge V\left(1-\cos(\theta_0)\right)+\frac{2\lambda_0}{T}. \end{aligned} \tag{21}$$

In this case, the contributions to the reverberation intensity come from the scatterers in the mainlobe of the beampattern, but at different frequencies. Reverberation is now suppressed by the spectral analysis (or Doppler filter), and the ratio of reverberation over signal power for WCW pulses in zone $\mathbf{C}$ now reads for Hamming and $\sin^2$ pulse shadings

$$\mathrm{RSR} \simeq \frac{1}{2}T2\theta_3 10^{-\frac{\mathrm{SSLL}}{10}} \tag{22}$$

where $2\theta_3 = 1.3(\lambda_0/L)$ is the $-3$-dB mainlobe beamwidth of an array of length $L$ with Hamming weighting and SSLL is the spectral sidelobe level. The Doppler filter is very effective in zone $\mathbf{C}$. Reverberation suppression is so powerful ($-50$ to $-60$ dB) that in almost any environment the performance becomes noise limited. In these cases, the detection performance increases with pulse length; this is in contrast to the detection performance in zone $\mathbf{B}$.

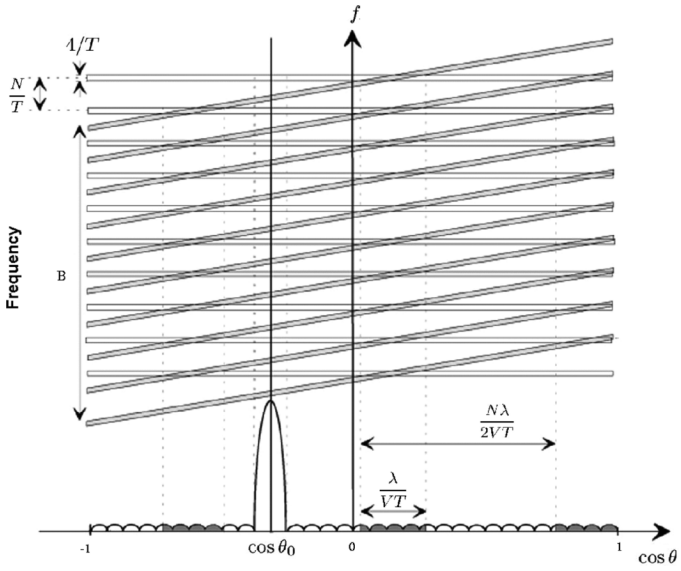


Fig. 6. Reverberation zones for a PTFM pulse.

### D. Wideband Comb Spectrum Signals

In this section, we assess the gain provided by a strategy combining Doppler rejection of reverberation and high bandwidth. For this purpose, we use a transmitted signal with a comb spectrum to get Doppler rejection as soon as the Doppler shift of the target is larger than the width of the spectral peaks. This comb spectrum is obtained by transmitting a train of wideband LFM pulses. The PTFM signal has a subpulse length $T_p$, bandwidth $B$, and central frequency $f_0$, and the total pulse train consists of $N$ subpulses. The total waveform can be described as

$$e(t) = \sum_{n=0}^{N-1} \sin^2\left(\pi \frac{n}{N}\right) p(t - nT_p)$$

where

$$p(t) = \exp\left(2\pi\imath t\left[f_0 + B\frac{t}{2T_p}\right]\right), \quad \text{for} \quad 0 \le t \le T_p = \tfrac{T}{N}. \quad (23)$$

In Fig. 6 (cf., [16]), the spectrum of a PTFM pulse is shown. This spectrum is a comb consisting of several lines at frequencies $f_m = m/T_p$, filtered by the spectrum of the base pulse in the bandwidth $f_0 - B/2 \le f_m \le f_0 + B/2$. Each of the $P \simeq BT_p$ spectral lines is convolved by the spectrum of the amplitude shading function $\sin^2(\pi t/T)$. As shown in the previous sections, the $-3$-dB spectral width for this kind of shading is $2/T$. The local spectral sidelobe level (i.e., between the spread spectral lines) is close to $-50$ dB, and can be controlled by altering the shading function.

For wideband comb spectrum signals, the concept of **A**, **B**, and **C** zones still holds. However, because of the comb spectrum of this pulse type, several directions (bearings) can contribute to the cross spectrum between the replica and reverberation. When using a cosine grid, these directions are spaced by $N\lambda_0/(2VT)$. The number of the overlaps in the cross spectrum between the replica and reverberation will be equal to

$$M = \text{ceil}\left(\frac{4VT}{N\lambda_0}\right) \quad (24)$$

or one more depending on the Doppler.

For zone **A**, other directions than the mainlobe are negligible, because they occur in the sidelobes of the beampattern. However, for zone **B**, these contributions add up to the total reverberation level. In the following subsections, the performance of the wideband comb spectrum signals is discussed for each reverberation zone.

*1) Zone* **A** *Performance:* In zone **A**, the cross spectrum between the replica and the reverberation falls in the mainlobe of the beam directivity pattern. From Fig. 6, it can be seen that this region corresponds to the following range of target radial speeds:

$$\begin{aligned}\left(1 + \frac{2V\cos(\theta_0)}{c} + \frac{2V_r}{c}\right) f_0 - \frac{2}{T} \\ \le \left(1 + \frac{2V\cos(\theta_0)^{(-)}}{c} + \frac{2V_r}{c}\right) f_0 + \frac{2}{T} \pm \frac{2kN}{T} \\ \left(1 + \frac{2V\cos(\theta_0)}{c} + \frac{2V_r}{c}\right) f_0 + \frac{2}{T} \\ \ge \left(1 + \frac{2V\cos(\theta_0)^{(+)}}{c} + \frac{2V_r}{c}\right) f_0 - \frac{2}{T} \pm \frac{2kN}{T} \end{aligned} \quad (25)$$

where $k$ is a nonnegative integer. However, for optimal performance in zone **B** (see next section), the pulse is designed in such a way that $k = 0$. In this case, (25) simplifies to (11), and the target speed range associated to zone **A** corresponds to the target speed range for a CW pulse in zone **A**

$$-V\frac{\beta\lambda_0}{L} - \frac{2\lambda_0}{T} \le V_r \le V\frac{\beta\lambda_0}{L} + \frac{2\lambda_0}{T}. \quad (26)$$

For a PTFM pulse with a $\sin^2$ shading, the signal power reads $S = (3T/8)^2$; see (12). The spectral energy is found from the peaks in the spectrum. As subpulses are linear FM pulses of duration $T_p$ and bandwidth $B$, we can approximate the square magnitude of their spectrum in their main band to $T_p/B$, and we get, from expression (23)

$$|E_0(f)|^2 \simeq \frac{T_p}{B}\left[\sum_{n=0}^{N-1} \sin^2\left(\pi\frac{n}{N}\right) e^{2\pi\imath f n T_p}\right]^2. \quad (27)$$

In the transmitted frequency band $B$, the spectrum has $P = BT/N$ peaks at frequencies $f_m = m/T_p$ of $-3$-dB width $2/T$ each. Square magnitude of the sprectum is given at those frequencies by

$$\left|E_0\left(\frac{m}{T_p}\right)\right|^2 \simeq \frac{T}{NB}\left(\frac{N}{2}\right)^2 = \frac{TN}{4B}. \quad (28)$$

The cross-spectrum term in (7) now becomes

$$\int_f |E_\theta(f)E_0(f)|^2 \,\mathrm{d}f = \left(\frac{TN}{4B}\right)^2 P\frac{1}{T} = \frac{NT^2}{16B}. \tag{29}$$

This results in the following expression for the RSR:

$$\mathrm{RSR} \simeq \frac{4}{9} 2\theta_3 \frac{N}{B}. \tag{30}$$

As for the CW case, a more accurate expression based on numerical evaluation of (12) and (13) yields for Hamming and $\sin^2$ pulse shadings

$$\mathrm{RSR} \simeq \frac{1}{2} 2\theta_3 \frac{N}{B}. \tag{31}$$

Reverberation to signal level of PTFM in zone $\mathbf{A}$ is the same as reverberation induced by $N$ FM pulses of the same total bandwidth. It is intermediate between HFM and WCW performances. In zone $\mathbf{B}$, performances will be improved by a Doppler rejection.

*2) Zone* $\mathbf{B}$ *Performance:* In zone $\mathbf{B}$, there are several directions where the replica spectra cross the reverberation spectra; see Fig. 6. Each of these directions adds to the total received reverberation intensity. The lower the number of subpulses becomes, the higher the number of crossovers is, so that the improvement brought by the reduction of the resolution cell is compensated by a corresponding increase in the number of directions contributing to reverberation in zone $\mathbf{B}$. However, we will restrict the discussion to the case $M \leq 1$ to avoid ambiguity in a Doppler measurement. Then, the best performance in zone $\mathbf{B}$ is obtained when $M = 1$, which corresponds to the number of subpulses

$$N = \frac{4VT}{\lambda_0} \quad \text{or} \quad P = \frac{B\lambda_0}{4V}. \tag{32}$$

In this case, the target radial speed associated to zone $\mathbf{B}$ is the same as for a CW pulse, and given by (16). The angular interval corresponding to the overlap between the replica and reverberation is now also the same as for a CW pulse and given by (18). Using (20) and (29) leads to the following expression for the RSR in zone $\mathbf{B}$:

$$\mathrm{RSR} \simeq \frac{1}{2}\frac{N}{B}\Delta\theta 10^{-\frac{\mathrm{SLL}}{10}}. \tag{33}$$

Compared to the zone $\mathbf{A}$ performance, we see that reverberation is reduced by the beamformer. The level is $P$ times lower than in the WCW case.

*3) Zone* $\mathbf{C}$ *Performance:* In zone $\mathbf{C}$, there is no scatter at the frequency of the target Doppler channel. This is the case for target radial speeds given by (21). Reverberation is now strongly suppressed by the Doppler filter (spectral analysis). The RSR for $\mathbf{C}$ zone now reads for Hamming and $\sin^2$ pulse shadings

$$\mathrm{RSR} \simeq \frac{1}{2}\frac{N}{B} 2\theta_3 10^{-\frac{\mathrm{SSLL}}{10}}. \tag{34}$$

The spectral sidelobe suppression is generally more than enough to push reverberation under the background noise in zone $\mathbf{C}$.

### *E. Wideband Flat Spectrum Signals*

Wideband flat spectrum signals are mostly used for detection of slowly moving targets. Today, the most commonly used wideband flat spectrum signal is the HFM pulse, also known as LPM pulse, as it is fully Doppler tolerant and allows to perform the matched filter with a single replica. The phase law of the HFM pulse is designed in such a way that the Doppler scaling of a target echo can be perfectly compensated for by a time lag of the replica, thus allowing to recover the correlation of the phase at the expense of a Doppler-delay ambiguity [12].

An HFM waveform can be described as

$$e(t) = \exp\left(2\pi\imath f_i T A \ln\left|A - \frac{t}{T}\right|\right)$$

with

$$A = \frac{f_f}{f_f - f_i}, \qquad \text{for} \quad 0 \leq t \leq T \tag{35}$$

where $f_i$ is the start frequency and $f_f$ is the stop frequency. The so-called envelope shading is applied to reduce the sidelobes in the range direction. With this type of shading, only the first and the last 5% of the pulse are shaded using a $\sin^2$ shading.

Because this pulse type is Doppler insensitive, the separation in zones $\mathbf{A}$, $\mathbf{B}$, and $\mathbf{C}$ does not hold anymore in a strict sense. However, one can say, in analogy with the Doppler-sensitive pulses, that zone $\mathbf{A}$ corresponds to the reverberation-limited case, which is investigated here.

*1) Performance (in All Zones):* For an unshaded HFM pulse, the signal power is $S = T^2$, which results in an almost flat signal spectrum within the transmission band

$$E_0(f) = \sqrt{T/B}. \tag{36}$$

In realistic situations (using an HFM pulse with a large $BT$ product), the transmitted bandwidth of an HFM pulse is much larger than the Doppler shift of the targets or reverberation (for instance, the Doppler shift of a target with a radial speed of 50 kn and a pulse center frequency of $f_0 = 1500$ Hz is 50 Hz compared to a typical pulse bandwidth of $B = 500$ Hz). In this case, the overlap between the replica spectrum and the reverberation spectrum is approximately $B$. The reverberation level at replica correlation output now becomes

$$\int_f |E_\theta(f)E_0(f)|^2 \,\mathrm{d}f \simeq \left(\frac{T}{B}\right)^2 B. \tag{37}$$

This results in the following expression for the RSR:

$$\mathrm{RSR} \simeq 2\theta_3 \frac{1}{B}. \tag{38}$$

Good performance against reverberation is expected for high bandwidth pulses. The result is independent of pulse duration.

### *F. Discussion*

The expressions derived in the previous sections are used in the next section to compute the theoretical gain of the different transmitted pulses in the three reverberation zones. In Table I, the ratios of reverberation over signal power for the different

TABLE I
RSR FOR CW, PTFM, AND HFM PULSES IN THREE REVERBERATION ZONES (* THESE RATIOS ARE CALCULATED SUPPOSING EQUAL BANDWIDTH AND CENTRAL FREQUENCIES). OPTIMAL PERFORMANCE IS OBTAINED BY USING $N$ AS DEFINED IN (28)

| codes \ zones | zone A | zone B | zone C |
|---|---|---|---|
| HFM | $2\theta_3 \dfrac{1}{B}$ | | |
| CW | $2\theta_3 \dfrac{T}{2}$ | $\Delta\theta \dfrac{T}{2} 10^{-\frac{SLL}{10}}$ | $2\theta_3 \dfrac{T}{2} 10^{-\frac{SSLL}{10}}$ |
| PTFM | $2\theta_3 \dfrac{N}{2B}$. | $\Delta\theta \dfrac{N}{2B} 10^{-\frac{SLL}{10}}$ | $2\theta_3 \dfrac{N}{2B} 10^{-\frac{SSLL}{10}}$ |
| PTFM/CW* | $\dfrac{1}{P} = \dfrac{N}{BT}$ | | |
| PTFM/HFM* | $\dfrac{N}{2}$ | $\dfrac{NL}{2.6VT \sin\theta_r} 10^{-\frac{SLL}{10}}$ | $\dfrac{N}{2} 10^{-\frac{SLL}{10}}$ |

pulses in the three zones are summarized (assuming Hamming shading of the array, Hamming or $\sin^2$ shading of the CW and PTFM pulses, and equal central frequencies).

## III. EXPERIMENT SETUP

During the NAT II trial, held in October 1999, the emphasis was on reverberation suppression with several new pulse types and new beamforming techniques. These experiments were conducted in the shallow waters of the Spanish coast near La Coruña. During these experiments, the CAPTAS V1 system (consisting of a powerful broadband transducer and a $16\lambda$ array) and a CAPTAS $32\lambda$ array of TNO were towed behind Her Netherlands Majesty Ship (HNLMS) Tydeman. A Dutch submarine of the Walrus class served as a target during the experiments. This submarine was equipped with an ICT 2010 transducer, which was used to localize the submarine during the experiments. Furthermore, HNLMS Mercuur was involved in the experiments. She towed the "Imca Marina" source during the experiments and acted as a second artificial target for testing the beamforming and matched-filter algorithms.

### A. Sailed Tracks

One of the experiments conducted during the NAT II trial was designed to compare the performance of the PTFM pulse against WCW and HFM pulses in a reverberation-limited environment. For this purpose, the submarine was sailing along the coast, above the uprising sea bottom, and the sonar was on the deep water side, so that strong reverberation was received at the same time as the target echo. During this experiment, the submarine sailed on the coastal side of HNLMS Tydeman at different courses and speeds in such a way that it always remained near broadside of HNLMS Tydeman. In this way the submarine had a different Doppler for each leg. The submarine speeds zero (0 kn), low (3.5 kn), and high (10 kn) correspond to reverberation zones **A**, **B**, and **C**, respectively. The actual sailed tracks of HNLMS Tydeman and the submarine are shown in Fig. 7.

The whole experiment consisted of 12 legs, which lasted 15 min each. At the end of each leg, the submarine changed course and speed in 5 min. HNLMS Mercuur sailed parallel to HNLMS Tydeman on the seaside at a constant range of 5 nmi

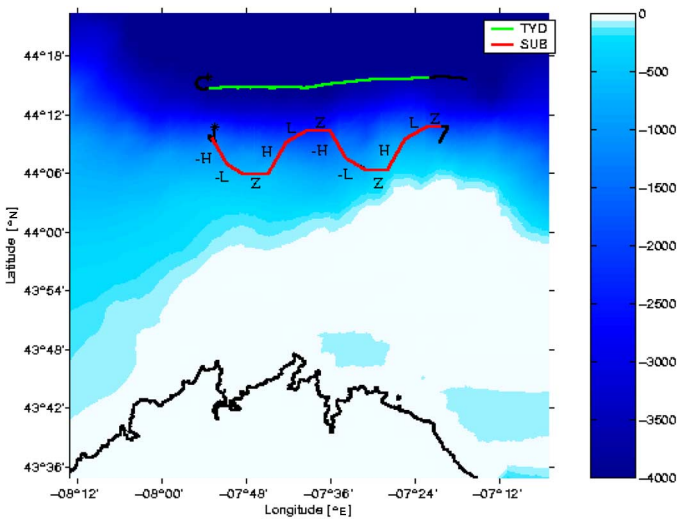


Fig. 7. Actual sailed tracks of HNLMS Tydeman and the submarine during the experiment (* denotes the start of the experiment). Depth color scale in meters.

and a portside bearing of 135° ($\cos\theta = -0.7$). Both surface ships sailed at a speed of 6 kn. During this experiment, the Sea State was about 3 with a moderate wind (10 m/s) from the east.

### B. Transmitted Pulses

During the experiment, several pulse types were transmitted to compare them under (almost) similar conditions. In the following subsections, the different pulses and their characteristics are described.

*1) CW Pulse:* Two CW pulses, at different frequencies, are transmitted directly after the PTFM pulse and are used for the comparison between the CW pulse and PTFM pulse. To avoid interference between the CW pulse and the PTFM pulse, the CW pulses are centered outside the frequency band of the PTFM at 1088 and 1919 Hz, respectively. The pulse duration of the two (Hamming weighted) CW pulses is 4 s.

In Fig. 2, the ambiguity function of the 1088-Hz (Hamming weighted) CW pulse is given. This ambiguity function shows the high Doppler resolution (the $-3$-dB resolution is 0.57 kn) of this pulse, however, at the expense of a very poor range resolution ($-3$-dB resolution is 1500 m).

*2) PTFM Pulse:* During the experiments, the PTFM pulses, centered at 1500 Hz, are transmitted by both HNLMS Mercuur and HNLMS Tydeman. The transmitted PTFM pulse consisted of 128 LFM subpulses with a total duration of 4 s. Each LFM subpulse (and, therefore, the total pulse) has a bandwidth of 700 Hz. To reduce Doppler sidelobes, the pulse is weighted according to (23), with Hamming coefficients instead of $\sin^2$ applied to subpulses. For comparison with the CW pulses, the PTFM pulse is followed directly by the two out of band CW pulses centered at 1088 and 1919 Hz. HNLMS Mercuur transmits this pulse every 60 s without any interruption. The PTFM transmission from HNLMS Tydeman is interleaved with an HFM pulse every fifth transmission for real-time localization of the submarine.

*3) HFM Pulse:* Both the submarine and HNLMS Tydeman transmit HFM pulses for an accurate localization of the submarine during the experiments. The high bandwidth of the HFM

TABLE II
THEORETICAL PROCESSING GAIN (IN DECIBELS) OF THE PTFM PULSE OVER THE CW AND HFM PULSES. (* NOTE THAT GAINS ARE SLIGHTLY DIFFERENT FROM THOSE OF ZONES A AND C DUE TO A DIFFERENT CENTRAL FREQUENCY BETWEEN THE PTFM PULSE AND THE CW PULSE)

| Pulse type | zone A | zone B | zone C |
|---|---|---|---|
| $\frac{PTFM}{CW1088}$ | 15 | $13^*$ | 15 |
| $\frac{PTFM}{CW1919}$ | 12 | $14^*$ | 12 |
| $\frac{PTFM}{HFM}$ | -14 | 13 | 34 |

pulse (500 Hz) results in a very high range resolution. This pulse also has a pulse duration of 4 s. The corresponding ambiguity function is shown in Fig. 1. The ambiguity function clearly shows the high range resolution and the insensitivity for target Doppler speed.

### C. Discussion

Based on a Hamming shaded $32\lambda$ array, we can compute the theoretical performance of the transmitted pulses in reverberation zones $\mathbf{A}$, $\mathbf{B}$, and $\mathbf{C}$. Because the performance in zone $\mathbf{B}$ strongly depends on the beamformer, sidelobe levels have been measured using the locator transmissions from HNLMS Mercuur; see the Appendix. In Table II, the expected gains of the PTFM pulse over the CW and HFM pulses are shown.

For an accurate estimation of the expected gains, the remark mentioned in Section II has to be accounted for. This remark stated that for zone $\mathbf{A}$, the angular width of the reverberation cell is governed by the product of the beampattern and the cross spectrum between reverberation and replica. The cross-spectrum effect will limit the reverberation cell to the scatterers entering the Doppler filter. We have assumed in the derivation of (15) that $L/VT \gg 1$, but with the trial parameters, this ratio is $22.68/12 = 1.89$, and an exact calculation based on (7) shows that theoretical reverberation of PTFM (and WCWs) is reduced by 2 dB with the parameters of the trials. This has been accounted for in Table II.

Table II clearly shows that the wideband PTFM pulse is expected to outperform both CW pulses in all three zones, with an expected gain of 12–15 dB. Compared to the HFM pulse reverberation, levels in zone $\mathbf{A}$ will be 14 dB higher, however in zone $\mathbf{B}$, a gain of 13 dB is expected. In Section IV, we will see if the PTFM pulse can fulfill these expectations.

## IV. REVERBERATION ANALYSIS

The reverberation analysis starts with the processing chain, which is used to process the acoustic data. Furthermore, a method is described to measure the reverberation in zones $\mathbf{A}$ and $\mathbf{B}$. The measured reverberation is then compared to the theoretical values found in Section III. This section concludes with a discussion on the measured reverberation levels.

### A. Processing of the Data

The processing of the acoustic data has been performed on the CAPTAS $32\lambda$ array. This array consists of 64 triplets, which enable P/S discrimination. However, in this paper, single array processing is applied, because the main emphasis is on reverberation suppression using new wideband Doppler-sensitive pulses, and not on the P/S rejection; this topic was treated in [3].

During the sea-trial, the acoustic data is received by the CAPTAS triplet array and saved on tape. This data is then sent to a sonar processor, which performs the following operations.

- One single line $32\lambda$ subarray is formed by selecting one sensor from each triplet. This subarray is beamformed using a delay and sum beamformer; see e.g., [2]. In total, 96 beams are formed in the cosine grid from $\cos\theta = -1$ to 1 (corresponding to $\pm 180°$).
- The beamformed data is matched filtered with several Doppler shifted replicas for the CW and PTFM pulses. For the CW and PTFM pulses, the replicas are spaced at 0.2 kn. The Doppler insensitive HFM pulse was matched filtered with one replica at zero knot.
- Processing is normalized with the transmitted energy (shading functions) corresponding to the theory of Section II.
- Corrections are made for frequency-dependent scaling factors in the data acquisition system and source level; see the Appendix.
- The matched-filtered data is saved to disk for further analysis.

### B. Analysis Method

Measuring the (bottom) reverberation levels in different zones is much more difficult than it seems at first glimpse. First, one has to be sure that the analyzed data is reverberation limited and that the scatterers are homogeneously distributed. A good overview of the scatterer distribution, in range and bearing, can be obtained using the HFM transmissions. In Fig. 8, four range-bearing plots of HFM transmissions are shown. These data are from the beginning, 1/3, 2/3, and the end of the experiment, respectively. The time between each figure is approximately 1 h.

At the beginning of the experiment, the reverberation between 2 and 10 nmi is distributed relatively homogeneously, where the lower limit is determined by the water depth. However, during the experiment, both the reverberation intensity and the distribution of the scatterers changes slowly. Analysis of all transmitted HFM pulses shows that the global reverberation intensity dropped almost 8 dB during the experiments. However, generally, the area between 4 and 5 nmi has a relatively constant and homogeneous scatterer distribution, both in range and bearing. Therefore, this area will be used for the reverberation analysis.

The average reverberation level is computed by averaging the intensity between 4 and 5 nmi for all bearings between 35° and 145° ($\cos\theta = -0.8$ and 0.8). Endfire beams are not used, because of very low-reverberation levels in this area (only volume scattering).

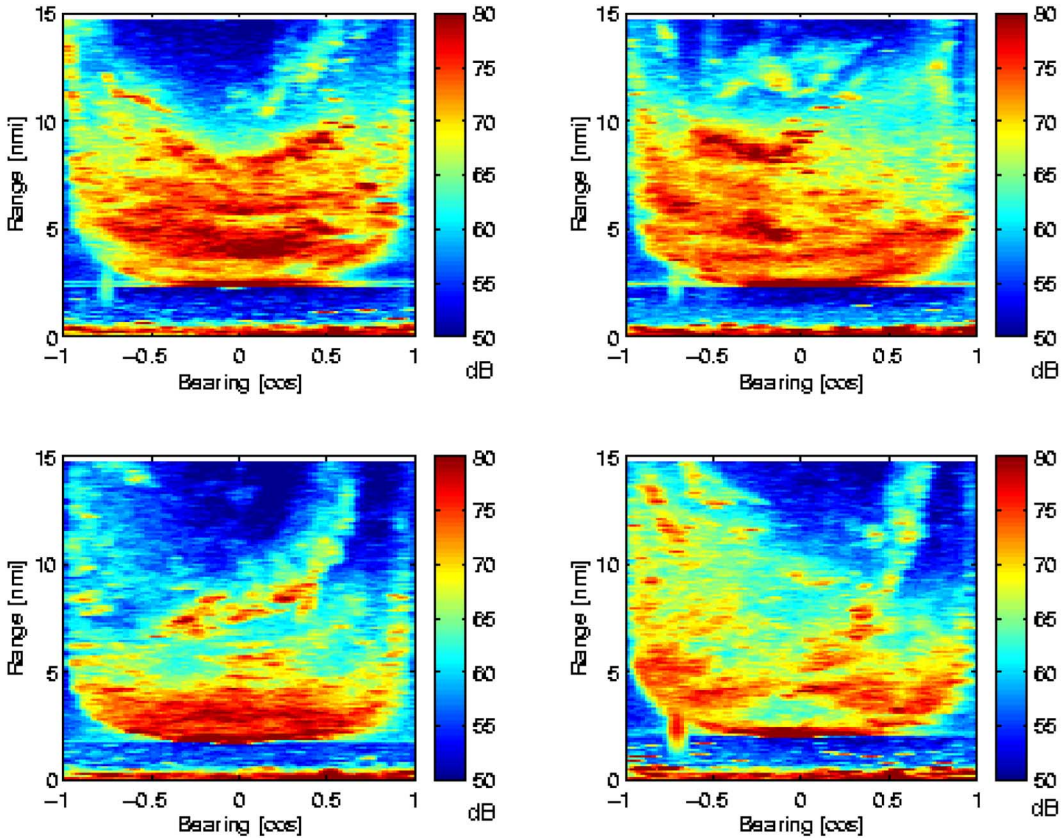


Fig. 8. Changing coastal (reverberation) structures during the experiment (clockwise the beginning of the experiment, 1/3, 2/3, and the end of the experiment) for the HFM pulse.

For the Doppler-sensitive CW and PTFM pulses, an additional dimension is available for the estimation of the reverberation levels, namely, the Doppler. However, by averaging the intensities over the same ranges as done for the HFM pulse, this is reduced to two dimensions. In the remaining two dimensions (bearing and Doppler), the reverberation levels can be estimated for zones $\mathbf{A}$ and $\mathbf{B}$. The measurement of the reverberation in zone $\mathbf{C}$ is not possible because we are always sea noise limited in this situation (reverberation suppression is too powerful here). An example of the three reverberation zones in a bearing–Doppler plot was given in Fig. 4.

The frequency shift (or Doppler) of the reverberation in zone $\mathbf{A}$ is determined by the tow speed and was given in (9). Using this equation and the 3-dB beamwidth, the reverberation level in zone $\mathbf{A}$ is computed by averaging the intensity. To avoid endfire beams, the measurement is limited to bearings between 35° and 145° ($\cos\theta = -0.8$ and 0.8). An example is given in Fig. 9, where the amplitudes in the black parallelogram are averaged to obtain the reverberation level in zone $\mathbf{A}$.

For zone $\mathbf{B}$, the area of interest was given by (16). Using this equation, the reverberation level is computed by averaging the intensities in this area. In this case, the measurements are limited to bearings between 35° and 145° ($\cos\theta = -0.8$ and 0.8) to avoid endfire beams. An example is given in Fig. 9, where the intensities in the two white triangles are averaged to obtain the reverberation level in zone $\mathbf{B}$.

Several remarks can be made from Fig. 9. First, when we compare the two CW pulses (one at 1088 Hz and the other at 1919 Hz), we see that the high-frequency pulse has a smaller zone $\mathbf{A}$ compared to the low-frequency pulse. The smaller $-3$ dB beamwidth and the higher Doppler resolution of the high-frequency pulse are the main causes. This results in slightly lower reverberation levels. Comparing the PTFM pulse with both CW pulses shows a significant reduction of the reverberation in zones $\mathbf{A}$ and $\mathbf{B}$.

### C. Analysis Results

In this section, a more statistical analysis of the processing gain of the PTFM pulse is given. For this analysis, all useful transmissions are used to measure the reverberation in zones $\mathbf{A}$ and $\mathbf{B}$. Transmissions that are contaminated with passive contacts or consist of bad data are not used. In total 137 transmissions with Doppler-sensitive pulses (combined CW and PTFM pulses) and 42 transmissions with HFM pulses are used for the analysis. In Fig. 10, the measured reverberation levels in zone $\mathbf{A}$ are shown for the four analyzed pulses. The data from the HFM pulse is interpolated to the corresponding transmissions of the Doppler-sensitive pulses.

Directly visible from Fig. 10 is the large difference between the HFM and Doppler-sensitive pulses. On average, the reverberation levels of the HFM pulse are approximately 15 dB lower than the PTFM one and 25 dB lower than the CW one. Also visible is the slow decrease of the reverberation levels during the experiment. Of the Doppler-sensitive pulses, the PTFM pulse outperforms both CW pulses, as expected.

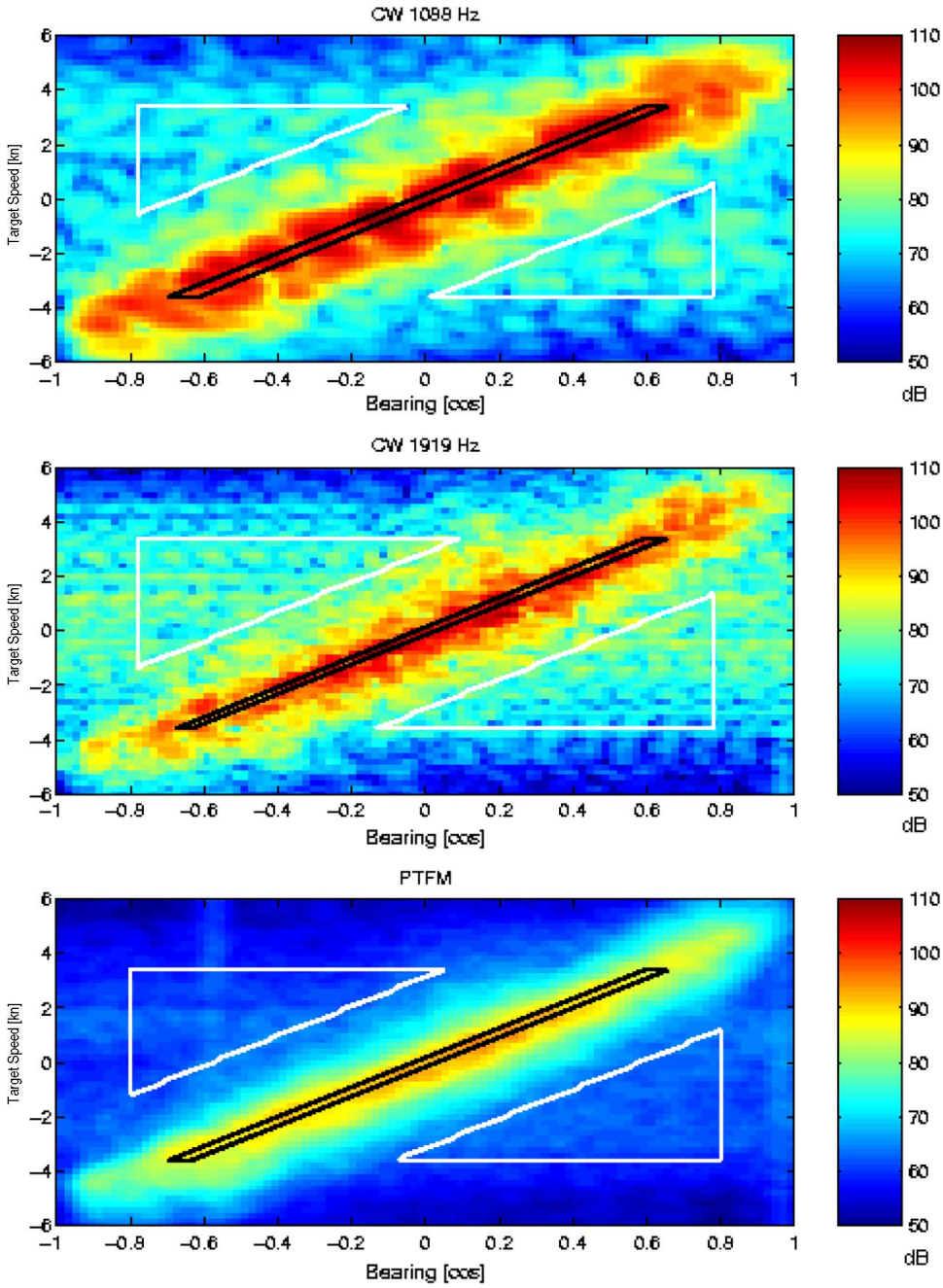


Fig. 9. Measurement of the reverberation in zone $\mathbf{A}$ (black box) and $\mathbf{B}$ (white box) for the low-frequency CW (top), high-frequency CW (middle), and PTFM (bottom) pulses.

The measured reverberation levels in zone $\mathbf{B}$ are shown in Fig. 11 for the four analyzed pulses. In this case, the PTFM pulse outperforms all three other pulses. The reverberation levels of the HFM pulse are now between the reverberation levels of both CW pulses. Again, we see that the average reverberation levels drop during the experiment.

Using Figs. 10 and 11, the gain of each pulse in zone $\mathbf{B}$ with respect to zone $\mathbf{A}$ can be computed. This is shown in Table III together with the standard deviation and the theoretical gain based on Table I and the measured sidelobe levels as shown in the Appendix. Also shown are the values for a "theoretical" 1500-Hz CW pulse to have a more direct comparison between the CW, HFM, and PTFM pulses. The reverberation levels for this pulse are obtained by averaging the reverberation levels of the 1088- and 1919-Hz CW pulses. No HFM results are shown in Table III, as the reverberation for this pulse does not depend on the Doppler zones $\mathbf{A}$, $\mathbf{B}$, or $\mathbf{C}$.

The average gain in zone $\mathbf{B}$ is, within statistical fluctuations, comparable to theory. Performance of the PTFM and CW pulses in reverberation zone $\mathbf{B}$ is mainly determined by the beampattern sidelobe level; see Table I. Improved array calibration decreases the sidelobe levels, which directly pays back in lower reverberation levels in zone $\mathbf{B}$.

Of greater practical interest is the gain of the PTFM pulse with respect to the other transmitted pulses. In Table IV, this gain is shown together with the expected (theoretical) gain.

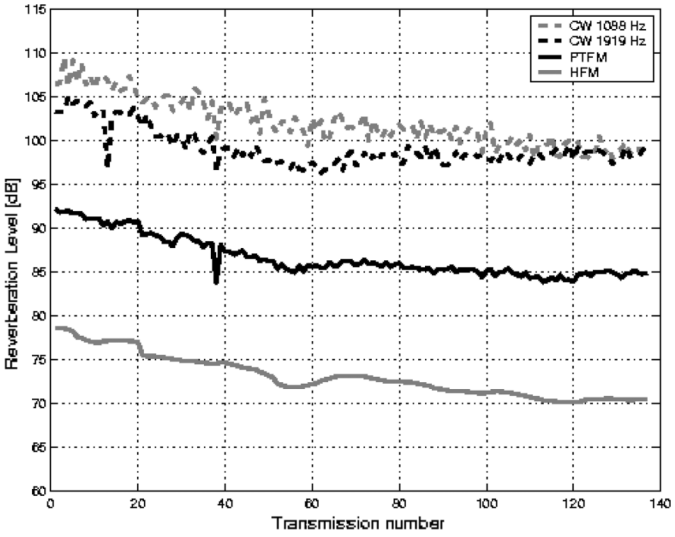


Fig. 10. Measured reverberation levels in zone **A** for the CW, PTFM, and HFM pulses.

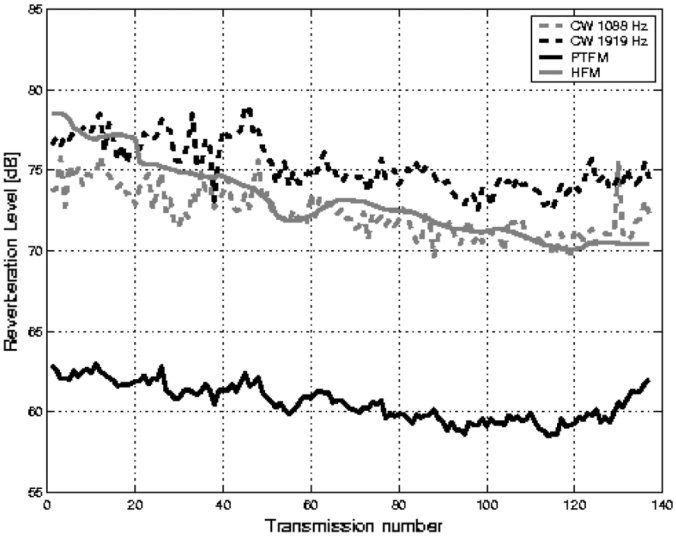


Fig. 11. Measured reverberation levels in zone **B** for the CW, PTFM, and HFM pulses.

TABLE III
MEASURED AND THEORETICAL REVERBERATION REDUCTION IN ZONE **B** WITH RESPECT TO ZONE **A**

| Pulse type | Measured reduction [dB] | Theoretical reduction [dB] |
|---|---|---|
| CW 1088 | 30.5 ± 1.7 | 30 |
| CW 1919 | 24.5 ± 1.5 | 26 |
| CW 1500 | 27.5 ± 1.3 | 28 |
| PTFM | 26.4 ± 1.4 | 28 |

Table IV shows that the measured gain of the PTFM matches the theoretical predictions. In zone **A**, the PTFM pulse outperforms both CW pulses. However, the HFM pulse performs better, because of the high range resolution of this pulse. In zone **B**, the PTFM pulse outperforms both the CW pulses and the HFM pulse.

TABLE IV
MEASURED AND THEORETICAL PROCESSING GAIN (BETWEEN BRACKETS) OF THE PTFM PULSE OVER THE CW AND HFM PULSES IN REVERBERATION-LIMITED AREAS

| pulse type | gain zone A [dB] | gain zone B [dB] |
|---|---|---|
| $\frac{PTFM}{CW\ 1088}$ | 15.5 ± 1.1 (15) | 11.4 ± 0.9 (13) |
| $\frac{PTFM}{CW\ 1919}$ | 12.5 ± 1.2 (12) | 14.3 ± 0.8 (14) |
| $\frac{PTFM}{CW\ 1500}$ | 14.0 ± 0.7 (13) | 12.9 ± 0.7 (13) |
| $\frac{PTFM}{HFM}$ | -13.7 ± 0.7 (-14) | 12.7 ± 1.3 (13) |

### *D. Discussion*

As can be seen from Table IV, the ratio of PTFM to WCWs reverberation levels measured in zone **A** is in good agreement with theory. This could be expected for two reasons:

- the three waveforms were transmitted in a combined transmission, so that they sample the reverberation in the same area;
- the theoretical value of the ratio only depends on known parameters, namely, pulse characteristics (duration, bandwidth, and shading) and frequency (for the angular width of the reverberation cell).

The ratio of PTFM to WCWs levels in zone **B** shows also a good agreement with theoretical predictions except perhaps for the case of WCW 1088 Hz. Larger discrepancies with theory could be explained by the fact that the reverberation levels in zone **B** depend on a sidelobe level, which is an estimated parameter of the system, and shows some variation ($\pm$1.5 dB) over the horizon, as can be seen from the beampatterns plotted in the Appendix.

The ratio of PTFM to HFM also shows good agreement with theory for zones **A** and **B**.

It should be remarked here that the HFM pulse does not have a flat spectrum over the transmitted bandwidth, while the PTFM pulse does because it consists of a train of linear FMs. The corresponding loss in reverberation is 0.4 dB with the HFM waveform parameters (ratio of PTFM to HFM lowered by 0.4 dB).

## V. CONCLUSION

In this paper, a comparison is made between the different types of detection pulses in an area with high reverberation levels, which originated from a steep slope. The target was positioned up-slope and sailed at different speeds, such that its Doppler was zero, low, and high, corresponding to the reverberation zones **A**, **B**, and **C**, respectively. The aim was to find the best pulses for zone **B**, i.e., slow moving targets, which is of great operational interest. In zones **A** and **C**, detection can be performed with standard (wideband flat spectrum) HFM and

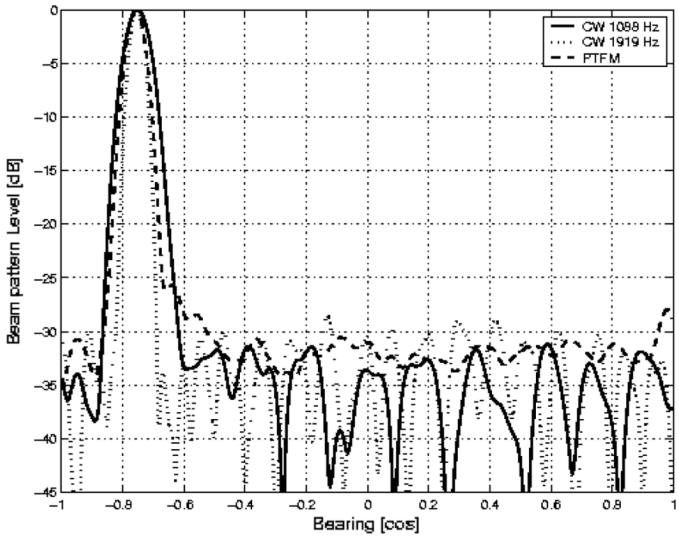


Fig. 12. Measured beampatterns for low- and high-frequency CW and PTFM pulses.

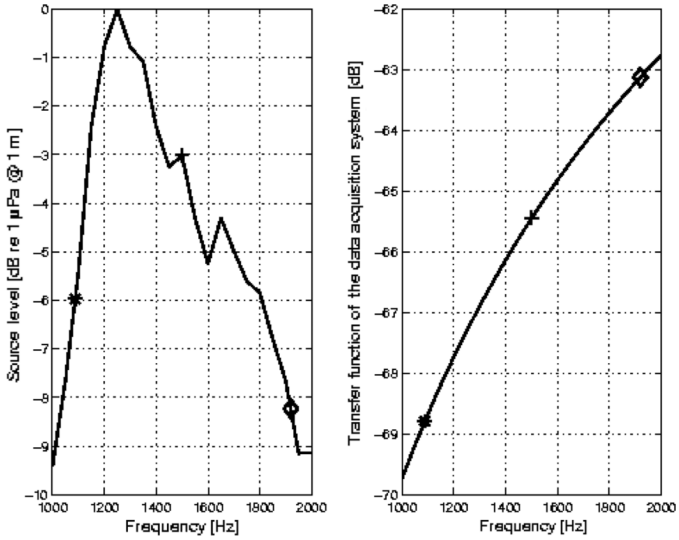


Fig. 13. Frequency-dependent correction curves for the source level (left) and data acquisition system (right). Center frequencies of low- and high-frequency CW pulses and PTFM/HFM pulses are depicted by $*$, $\diamond$, and $+$, respectively.

(narrowband) CW pulses, respectively. However, for zone $\mathbf{B}$, a new type of PTFM pulses with a wideband comb spectrum is proposed.

Theoretically, it is shown that for typical LFAS scenarios, wideband PTFM pulses have a gain over CW and HFM pulses of about 13 dB in zone $\mathbf{B}$, under the assumption that the receiving array is well calibrated. Especially, the zone $\mathbf{B}$ performance is sensitive to the sidelobes and array shading is required. Array calibration is, therefore, an important issue.

Analysis of the experiments with different pulses in different reverberation showed good results, which are compliant to the presented theory. The gain over CW pulses was on average 11–15 dB with 1-dB uncertainty, which is a closely matching theory. Compared to the HFM pulse in zone $\mathbf{A}$, this pulse is still preferable with an average gain of 14 dB with 1-dB uncertainty. However, as expected, the gain over HFM was 13 dB in zone $\mathbf{B}$.

Here, it should be noted that the PTFM performance was not optimal during these experiments. The transmitted pulse consisted of 128 subpulses, which could have been reduced to 48 according to (32), which would have increased the performance with another 4 dB in zone $\mathbf{B}$.

## APPENDIX

For a correct estimation of the theoretical gain in zone $\mathbf{B}$, the sidelobe levels after beamforming are very important. Theoretical computation of the sidelobe levels is possible. However, "real life" effects such as phase errors have a great influence on this level. Therefore, the actual sidelobe levels are estimated using the locator transmissions from HNLMS Mercuur. These locator transmissions have the advantage of a high SNR, so that an accurate estimation can be done.

In Fig. 12, an example is given for the low- and high-frequency CW pulses and the PTFM pulse.

From this figure, the sidelobe levels shown in Table V are used for the computation of the theoretical gain in zone $\mathbf{B}$.

TABLE V
MEASURED SIDELOBE LEVELS. *THE SIDELOBE LEVEL FOR THE 1500-Hz CW IS THE AVERAGE VALUE OF THE LOW- AND HIGH-FREQUENCY CWS

| Pulse type | side-lobe level [dB] |
|---|---|
| CW 1088 | -34 |
| CW 1919 | -30 |
| CW 1500* | -32 |
| PTFM | -32 |

For a good comparison between the different pulses all scaling factors have to be compensated for. Scaling of the beamformer, matched filter, etc., is integrated in the processing. However, two other scaling factors remain, namely, the effects of the transmitted source level and the transfer function of the data acquisition system in the array, consisting of a prewhitening filter and amplifiers. Both effects are frequency dependent and cannot be neglected. In Fig. 13, these effects are shown. On the left-hand side, the level of the sound source is shown versus frequency, and on the right-hand side, the transfer function of the acquisition system is shown in the active frequency band.

Using these two curves, the absolute reverberation levels of the different pulses can be computed and compared.

## REFERENCES

[1] R. J. Urick, *Principles of Underwater Sound*. New York: McGraw Hill, 1975, p. 237.
[2] R. O. Nielsen, *Sonar Signal Processing*. Norwood, MA: Artech House, 1991, ch. 2.
[3] J. Groen, S. P. Beerens, R. Been, Y. Doisy, and E. Noutary, "Adaptive port-starboard beamforming of triplet sonar arrays," *IEEE J. Ocean. Eng.*, vol. 30, no. 2, pp. 348–359, Apr. 2005.
[4] B. Harris and S. A. Kramer, "Asymptotic evaluation of the ambiguity functions of high-gain FM matched filter sonar systems," *Proc. IEEE*, vol. 56, no. 12, pp. 2149–2157, Dec. 1968.
[5] Z. B. Lin, "Wideband ambiguity function of broadband signals," *J. Acoust. Soc. Amer.*, vol. 83, no. 6, pp. 2108–2116, 1988.
[6] Y. Doisy, L. Deruaz, S. P. Beerens, and R. Been, "Target Doppler estimation using wideband frequency modulated signals," *IEEE Trans. Signal Process.*, vol. 48, no. 5, pp. 1213–1224, May 2000.

[7] G. Jourdain and J. P. Henrioux, "Use of large bandwidth-duration binary phase shift keying signals in target delay Doppler measurements," *J. Acoust. Soc. Amer.*, vol. 90, no. 1, pp. 299–309, July 1991.
[8] S. A. Kramer, "Statistical analysis of wide-band pseudorandom matched filter sonars," *IEEE Trans. Aerosp. Electron. Syst.*, vol. AES-5, no. 4, pp. 152–155, Jul. 1969.
[9] T. Collins and P. Atkins, "Nonlinear frequency modulation chirps for active sonar," *Inst. Electr. Eng. Proc. Radar Sonar Navigat.*, vol. 146, no. 6, pp. 312–316, 1999.
[10] J. P. Costas, "A study of a class of detection waveforms having nearly ideal range-Doppler ambiguity," *Proc. IEEE*, vol. 72, no. 8, pp. 996–1009, Aug. 1984.
[11] S. A. Kramer, "Doppler and acceleration tolerances of high-gain, wide-band linear FM correlator sonars," *Proc. IEEE*, vol. 55, no. 7, pp. 627–636, Jul. 1967.
[12] J. J. Kroszczinski, "Pulse compression by means of linear-period modulation," *Proc. IEEE*, vol. 57, no. 7, pp. 1260–1266, Jul. 1969.
[13] H. Cox and H. Lai, "Geometric Comb waveforms for reverberation rejection," in *Proc. 29th Asilomar Conf. Signals Syst. Comput.*, Pacific Grove, CA, 1995, pp. 1185–1189.
[14] T. Collins and P. Atkins, "Doppler-sensitive active sonar pulse design for reverberation processing," *Inst. Electr. Eng. Proc. Radar Sonar Navigat.*, vol. 145, no. 6, pp. 347–353, 1998.
[15] T. Collins, "Active sonar pulse design," Ph.D. dissertation, School Eng., Univ. Birmingham, Birmingham, U.K., 1996.
[16] Y. Doisy, L. Deruaz, and R. Been, "Sonar waveforms for reverberation rejection part I: Theory," in *Proc. Undersea Defense Technol. Pacific*, 2000, pp. 19–24.
[17] R. Been, S. P. Beerens, S. P. van IJsselmuide, and B. Prunel, "Sonar waveforms for reverberation rejection part II: Experimental results," in *Proc. Undersea Defense Technol. Pacific*, 2000, pp. 25–29.
[18] Y. Doisy, L. Deruaz, B. Prunel, S. P. Beerens, and S. P. van IJsselmuide, "Sonar waveforms for reverberation rejection part III: More experimental results," in *Proc. Undersea Defense Technol. Eur.*, 2000, Session 6A.2.
[19] W. S. Burdic, *Underwater Acoustic System Analysis*. Englewood Cliffs, NJ: Prentice-Hall, 1984, p. 357.
[20] H. L. Van Trees, *Optimum Array Processing*. New York: Wiley-Interscience, 2002, p. 103.
[21] D. J. Ramsdale and R. A. Howerton, "Effect of element failure and random errors in amplitude and phase on the sidelobe level attainable with a linear array," *J. Acoust. Soc. Amer.*, vol. 68, no. 3, pp. 901–906, 1980.

**Yves Doisy** was born on September 9, 1958, in Soissons, France. He received the degree from Ecole Supérieure de Physique et Chimie Industrielles de la Ville de Paris (ESPCI), France, in 1983, and the M.S. degree in physical chemistry from University of Michigan, Ann Arbor, in 1985.

From 1986 to 1989, he did government sponsored research on signal processing for mine hunting sonars at Thomson Sintra ASM, Brest, France. He joined Thales Underwater Systems SAS (former Thomson Sintra ASM), Sophia-Antipolis, France, in 1989, where he was Head of the Signal Processing Laboratory from 1994 to 1998. He has been involved in applied research in the fields of active and passive sonar detection, localization and tracking, acoustic noise analysis, sonar simulation, and acoustic navigation. He has been appointed head of General Sonar Studies Department in 1999, covering research and development studies in the fields of sonar signal processing and underwater environmental modeling. He analyzed the theoretical performances of sonar waveforms and designed their parameters for the experimental assessment.

**Laurent Deruaz** was born in 1964 in Grenoble, France. He received a diploma from Ecole Supérieure d'Electricité (ESE), Paris, France, in 1987 and a Diplôme d'Etudes Approfondies in particle physics in 1988.

He joined Thomson Marconi Sonar, France, in 1990 where after two years of developing and validating a specific sonar, he led a series of studies in maneuvering TMA, array self-calibrating, high-order statistics, active pulses designing, and track before detect processing. After participating in the New Array Technology (NAT) program, he led the General Sonar Study team in Thales Underwater System Australia for five years. He now leads a group in the General Sonar Study service in Thales Underwater System, Sophia-Antipolis, France. His main interest is the signal processing of active sonar.

**Sander P. van IJsselmuide** received the B.Eng. degree in applied physics from the TH Rijswijk, The Hague, The Netherlands, in 1998.

Since 1998, he has been a Scientist at the Underwater Technology Department, The Netherlands Organization for Applied Scientific Research (TNO) Defence, Security and Safety, The Hague, The Netherlands. His main interest is the signal processing of low-frequency active and passive sonars.

**S. Peter Beerens** received the M.Sc. degree in theoretical physics from the University of Amsterdam, Amsterdam, The Netherlands, in 1990 and the Ph.D. degree from Utrecht University, Utrecht. The Netherlands, in 1995, for studies on *chaotic mixing in tidal areas* at the Netherlands Institute for Sea Research.

Since 1996, he has been a Scientist at the Underwater Technology Department, The Netherlands Organization for Applied Scientific Research (TNO) Defence, Security and Safety, The Hague, The Netherlands, where he is a Program Manager for research related to sonar systems. His main interest is the signal processing of low-frequency active sonars.

**Robert Been** received the M.Sc. degree in applied mathematics from Delft University of Technology, Delft, The Netherlands, in 1990.

From 1990 to 1993, he was a Scientist in the Signal Processing Group, Physics and Electronics Laboratory, The Netherlands Organization for Applied Scientific Research (TNO), The Hague, The Netherlands. From 1993 to 2000, he was a Scientist in what is currently known as the Underwater Technology Department of TNO Defence, Security and Safety, where he was the Program Manager for low-frequency active sonar research. From 2000 to 2006, he was a Senior Engineer in the Advanced Sonar Studies Department, Thales Underwater Systems, Sophia-Antipolis, France. In 2006, he joined NATO Undersea Research Centre (NURC), La Spezia, Italy, where he is a Principal Scientist and a Program Manager for antisubmarine warfare related research.